AD-A083 073 ARMY MISSILE COMMAND REDSTONE ARSENAL AL GROUND EQU--ETC F/G 14/5
STRESS INTENSITIES AROUND TRANSVERSE SURFACE FLAWS IN CYLINDRIC--ETC(U)
OCT 79 J A SCHAEFFEL

UNCLASSIFIED DRSMI/RL-80-1 NL

1 OF 1
AD A083073

END
DATE
FILMED
5-80
DTIC

ADA083073

(12)

LEVEL

TECHNICAL REPORT RL-80-1

STRESS INTENSITIES AROUND TRANSVERSE SURFACE FLAWS IN CYLINDRICAL SHELLS BY PHOTOELASTIC STRESS FREEZING

John A. Schaeffel, Jr.
Ground Equipment and Missile Structures Directorate
US Army Missile Laboratory

1 October 1979

U.S. ARMY MISSILE COMMAND
Redstone Arsenal, Alabama 35809

Approved for public release; distribution unlimited.

SMI FORM 1021, 1 JUL 79 PREVIOUS EDITION IS OBSOLETE

DISPOSITION INSTRUCTIONS

DESTROY THIS REPORT WHEN IT IS NO LONGER NEEDED. DO NOT RETURN IT TO THE ORIGINATOR.

DISCLAIMER

THE FINDINGS IN THIS REPORT ARE NOT TO BE CONSTRUED AS AN OFFICIAL DEPARTMENT OF THE ARMY POSITION UNLESS SO DESIGNATED BY OTHER AUTHORIZED DOCUMENTS.

TRADE NAMES

USE OF TRADE NAMES OR MANUFACTURERS IN THIS REPORT DOES NOT CONSTITUTE AN OFFICIAL ENDORSEMENT OR APPROVAL OF THE USE OF SUCH COMMERCIAL HARDWARE OR SOFTWARE.

14 DRSMI/RL-80-1

UNCLASSIFIED

SECURITY CLASSIFICATION OF THIS PAGE (When Data Entered)

REPORT DOCUMENTATION PAGE

READ INSTRUCTIONS BEFORE COMPLETING FORM

1. REPORT NUMBER: RL-80-1

2. GOVT ACCESSION NO.:

3. RECIPIENT'S CATALOG NUMBER: 9

4. TITLE (and Subtitle): 6 STRESS INTENSITIES AROUND TRANSVERSE SURFACE FLAWS IN CYLINDRICAL SHELLS BY PHOTOELASTIC STRESS FREEZING.

5. TYPE OF REPORT & PERIOD COVERED: Technical Report.

6. PERFORMING ORG. REPORT NUMBER:

7. AUTHOR(s): 10 John A. Schaeffel, Jr.

8. CONTRACT OR GRANT NUMBER(s):

9. PERFORMING ORGANIZATION NAME AND ADDRESS:
Commander
US Army Missile Command
ATTN: DRSMI-RLA
Redstone Arsenal, Alabama 35809

10. PROGRAM ELEMENT, PROJECT, TASK AREA & WORK UNIT NUMBERS: 12 41

11. CONTROLLING OFFICE NAME AND ADDRESS:
Commander
US Army Missile Command
ATTN: DRSMI-RPT
Redstone Arsenal, Alabama 35809

12. REPORT DATE: 11 1 Oct 1979

13. NUMBER OF PAGES: 50

14. MONITORING AGENCY NAME & ADDRESS (if different from Controlling Office):

15. SECURITY CLASS. (of this report): UNCLASSIFIED

15a. DECLASSIFICATION/DOWNGRADING SCHEDULE:

16. DISTRIBUTION STATEMENT (of this Report):
Approved for public release; distribution unlimited.

17. DISTRIBUTION STATEMENT (of the abstract entered in Block 20, if different from Report):

18. SUPPLEMENTARY NOTES:

19. KEY WORDS (Continue on reverse side if necessary and identify by block number):

Stress Intensity	Fringe Order
Stress Freezing	Transverse Crack
Photoelastic	Birefringent
Isochromatic	Combined Loading
Part Circular Flaw	

20. ABSTRACT (Continue on reverse side if necessary and identify by block number):

This report documents a set of seven tests for the determination of K_I stress intensity factors for isotropic cylinders with transverse part-circular cracks loaded in combined uniaxial extension and internal pressure. Part-circular cracks were machined into birefringent Hysol CP5-4290 photoelastic cylinders. The cylinders were then subjected to combined loading while in a stress freezing cycle. Slices of the cracks were made at various angles and analyzed with a photoelastic polariscope. A least-squares curve fit of the photoelastic data was used to generate K_I stress intensity factors.

DD FORM 1473, 1 JAN 73 — EDITION OF 1 NOV 65 IS OBSOLETE

UNCLASSIFIED

SECURITY CLASSIFICATION OF THIS PAGE (When Data Entered)

UNCLASSIFIED
SECURITY CLASSIFICATION OF THIS PAGE(When Data Entered)

~~20.~~ K_I data are plotted versus slice angle into the crack for various crack parameters. The results of the tests were compared with the results of previous tests in which the cylinders were loaded in either pure uniaxial tension or internal pressure.

UNCLASSIFIED
SECURITY CLASSIFICATION OF THIS PAGE(When Data Entered)

CONTENTS

ILLUSTRATIONS

ILLUSTRATIONS (Concluded).

PRECEDING PAGE BLANK-NOT FILMED

I. INTRODUCTION

This work is a continuation of the efforts of Mullinix and Smith [1] and Vandiver et al. [2]. Their work involved the determination of stress intensity factors for homogeneous cylinders loaded under one of three conditions: internal pressure, bending, extension and having part circular longitudinal or transverse cracks in the outer wall. The present work considers the problem of finding stress intensity factors under the combined loading action of internal pressurization and extension. Transverse flaws in cylinders were considered for this effort.

Although flaws on the surface of cylinders usually occur as semi-elliptical in shape, the flaws in this work had to be made mechanically. This was accomplished by cutting part-circular flaws with circular saw blades to simulate an elliptical crack. The approximation has been made before and does not appear to offer any serious error. In this effort the assumed stress field at the crack tip border is defined as a 50-50 stress mixture derived from internal cylinder pressurization and extensional loading. Fifty percent of the applied stress was obtained from internal pressurization while the remaining fifty percent was obtained from extension.

II. THEORY

The geometry for the part-circular transverse flaw may be described by the intersection of a circular element representing the flaw boundary with a hollow cylinder. *Figures 1* and *2* illustrate this geometry. For the opening mode of deformation, the stress distribution near the part-circular crack and in a plane perpendicular to the crackfront is given as [3,4,5]

$$\sigma_n = \frac{K_I}{(2\pi r)^{\frac{1}{2}}} \cos\frac{\psi}{2} \left\{ 1 - \sin\frac{\psi}{2} \sin\frac{3\psi}{2} \right\} \qquad (1)$$

$$\sigma_y = \frac{K_I}{(2\pi r)^{\frac{1}{2}}} \cos\frac{\psi}{2} \left\{ 1 + \sin\frac{\psi}{2} \sin\frac{3\psi}{2} \right\}$$

$$\tau_{ny} = \frac{K_I}{(2\pi r)^{\frac{1}{2}}} \sin\frac{\psi}{2} \cos\frac{\psi}{2} \cos\frac{3\psi}{2}$$

In Equation (1), K_I is the stress intensity factor and the coordinates for the crack border are shown in *Figure 3*. The effect on the stress field of the crack border curvature as well as the

location and shape of other boundaries is reflected in the magnitude of K_I, the stress intensity factor. It is assumed that the stresses singular in r are much larger than terms regular in r very near the crack tip. Since experimental measurements must be made away from the crack tip where regular terms may make a significant contribution to the total stress field then another way of determining K_I must be found. Irwin [6] developed an approximation for the regular terms by assuming a uniform stress field, σ_{on}, was superimposed at the crack tip and parallel to the crack plane. With his approximation the local stress field is given as

$$\sigma_n = \frac{K_I}{(2\pi r)^{\frac{1}{2}}} \cos\frac{\psi}{2}\left\{1 - \sin\frac{\psi}{2}\sin\frac{3\psi}{2}\right\} - \sigma_{on} \tag{2}$$

$$\sigma_y = \frac{K_I}{(2\pi r)^{\frac{1}{2}}} \cos\frac{\psi}{2}\left\{1 + \sin\frac{\psi}{2}\sin\frac{3\psi}{2}\right\}$$

$$\tau_{ny} = \frac{K_I}{(2\pi r)^{\frac{1}{2}}} \sin\frac{\psi}{2}\cos\frac{\psi}{2}\cos\frac{3\psi}{2}$$

σ_{on} does not affect the singular stress field but does alter the isochromatic fringe pattern which is proportional to the maximum in-plane shearing stress. The maximum shearing stress, τ_{max}, is usually determined readily from photoelasticity.

From Irwin's stress equations, the maximum shearing stress in the plane perpendicular to the crack front, y-n, can be obtained from

$$\tau_{max}^2 = \frac{(\sigma_n - \sigma_y)^2}{2} + \tau_{ny}^2 \tag{3}$$

as

$$\left\{2\,\tau_{max}\right\}^2 = \left\{\frac{K_I}{(2\pi r)^{\frac{1}{2}}}\sin\psi + \sigma_{on}\sin\frac{3\psi}{2}\right\}^2 + \left\{\sigma_{on}\cos\frac{3\psi}{2}\right\}^2 \tag{4}$$

In photoelasticity, the maximum shearing stress from the stress optic law is

$$\tau_{max} = \frac{fN}{2t} \tag{5}$$

where,

$t \equiv$ thickness of the specimen measured parallel to the direction of light propagation.
$N \equiv$ isochromatic fringe order.
$f \equiv$ photoelastic fringe constant of the material.

In practice, τ_{max}, is measured along the line $\psi = \pi/2$ where the maximum shearing stress is known to be large. Simplification of Equation (4) with $\psi = \pi/2$ results in the equation

$$4\,\tau_{max}^2 = \frac{K_I^2}{2\pi r} + \left\{\frac{K_I}{(\pi r)^{\frac{1}{2}}}\right\}\sigma_{on} + \sigma_{on}^2 \tag{6}$$

Only the stress intensity factor K_I is used in fracture criteria. Smith et al. [7] found that by solving Equation (6) for τ_{max} and truncating the results to the same order in r as Equation (2) that

$$\tau_{max} = \frac{K_I}{\sqrt{8\pi r}} + \sigma_{on} \tag{7}$$

If an apparent value of K, K_{ap} is defined as,

$$K_{ap} = \sqrt{8\pi r}\;\tau_{max}\;, \tag{8}$$

then Equation (7) can be written as

$$K_{ap} = K_I + \sqrt{8\pi r}\;\sigma_{on} \tag{9}$$

Equation (9) shows that in the region dominated by the singular stresses that there is a linear relationship between the apparent K and the square root of r. In determining K_I, the values of K_{ap} are plotted versus $r^{1/2}$ for a photoelastic slice specimen. Data points which fall on a straight

line are selected while all others are rejected. A least-squares straight-line curve fit is then given to the selected points and the value of K_I is determined by taking the value of K_{ap} at $r = 0$, since $K_{ap} = K_I$ at $r = 0$. *Figure 4* gives an example for a typical photoelastic slice specimen.

For clarity, the results of this experimental effort are compared with those of Reference [2]. To compute the overall stress level for experimentally subjecting a cylinder, Reference [5] was consulted. Thresher and Smith generated graphs of stress intensity factors for surface cracks in finite solids. Using their information along with the maximum allowable working stress in the photoelastic material a determination of σ_m, the nominal cylinder-wall stress, was made. From, σ_m, the maximum working internal pressure P_i of the cylinder was obtained from

$$P_i = \frac{T}{R_c}\sigma_m \tag{10}$$

where

T = Wall thickness of the cylinder.
R_C = Radius of cylinder measured to the center of the cylinder wall.

For the case of *pure internal pressure loading of a cylinder* reported in [2],

$$P_i = 2\frac{T}{R_c}\sigma_m \tag{11}$$

To compute the extensional loading P for the cylinder with a 50-50 stress mixture,

$$P = \frac{1}{2}\sigma_m A_c \tag{12}$$

while for the case reported for pure extensional loading in [2],

$$P = \sigma_m A_c \tag{13}$$

All stress levels were comparable since their ultimate determination was from the same source, Thresher and Smith [5].

III. EXPERIMENTATION

The determination of stress intensity factors for cylinders loaded in internal pressure and extension followed the work given in References [1] and [2] which used three dimensional

photoelasticity. A series of seven combined loading tests were performed. The photoelastic material, Hysol CP5-4290, was cast by the Hysol Corporation, Olean, New York, and used in the experimentation. The cylinders are nominally 5.875 inch in outside diameter with a 0.75-inch wall thickness. All the specimens had flaws oriented transverse to the cylinder axis. These flaws were machined with a circular saw blade 0.006-inch thick. Blade radii of 0.875 and 1.500 inch were used to produce flaws of two different sizes.

For the seven tests, the internal pressure and extension loads were determined using Equations (10) and (12). *Figure 5* illustrates the apparatus for generating the internal gas pressure and extensional loading. The uniform tension load was supplied by hanging dead weights on the cylinder. The internal pressure load was supplied by compressed air passing through a regulator. The gas pressure was measured by a Mercury manometer.

After the surface flaw was machined, the cylinder was annealed by thermal soaking at 280 degrees Fahrenheit for six hours followed by cooling at the rate of one degree Fahrenheit per hour. The stress freezing of the models was accomplished using the same thermal cycle as for annealing except under loading conditions. After the stress freezing cycle, slices perpendicular to the crack border were removed from the model by means of band saw. *Figure 6* illustrates a few of the various angles at which slices were taken. The number of slices varied from test to test depending on the flaw size. Each slice was polished with sandpaper. The CP5-4290 material's fringe constant was obtained from previous beam tests.

To improve resolution for analysis, slices were placed in an oil bath consisting of 75.5 percent by volume of Halowax oil and 24.5 percent mineral oil. Since the indices of refraction of the oil and CP5-4290 were the same, light scatter was minimized. The slices were observed in a comparator polariscope at 10X magnification.

By means of an XY-table on the polariscope, points on the slices could be located to within ±0.0001 inch. Fractional fringe orders were obtained using Tardy compensation.

IV. RESULTS AND DISCUSSION

The specimen test parameters and dimensions for the combined uniaxial tension and internal pressure loading tests are indicated in *Table 3*. *Tables 1* and *2* were reproduced from Reference [2] for comparison purposes and are for the separate loading cases. *Figures 7-10* are graphs of the non-dimensional stress intensity factor versus slice angle for transverse flawed cylinders loaded either in uniaxial tension or internal pressure. *Figures 11-17* are graphs of the non-dimensional stress intensity factor versus slice angle for transverse flawed cylinders

loaded in combined uniaxial tension and internal pressure. The combined loading case data compares favorably with the separate uniaxial and internal pressure load cases. In general, the data follows the same experimental trends and the stress intensity factors obtained for the combined loading case falls within the range of the individual load cases.

V. SUMMARY AND CONCLUSIONS

A series of seven separate tests were conducted in which part circular flaws simulating natural elliptical cracks were machined into Hysol CP5-4290 cylinders. The cylinders were subjected to combined internal pressure and uniaxial tension loading. A photoelastic stress freezing cycle was conducted for each cylinder. Following the stress freezing cycle each cylinder was sliced and analyzed using a polariscope with Tardy compensation. The stress intensity factors were shown plotted versus slice angle and were compared with a previous set of tests reported in Reference [2] The results indicate that the more complicated combined loading case produces results comparable to the separate loading cases. It appears that linear superposition of solutions for each stress intensity factor case (i.e., uniaxial loading or internal pressure loading) is valid.

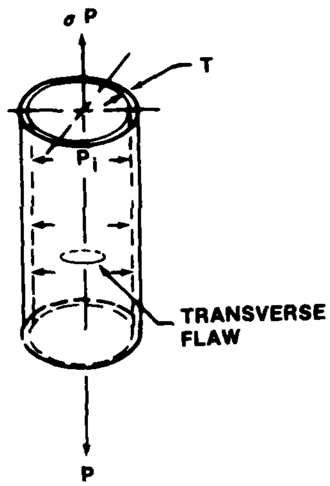

Figure 1. Transverse flaw loading geometry for a hollow cylinder.

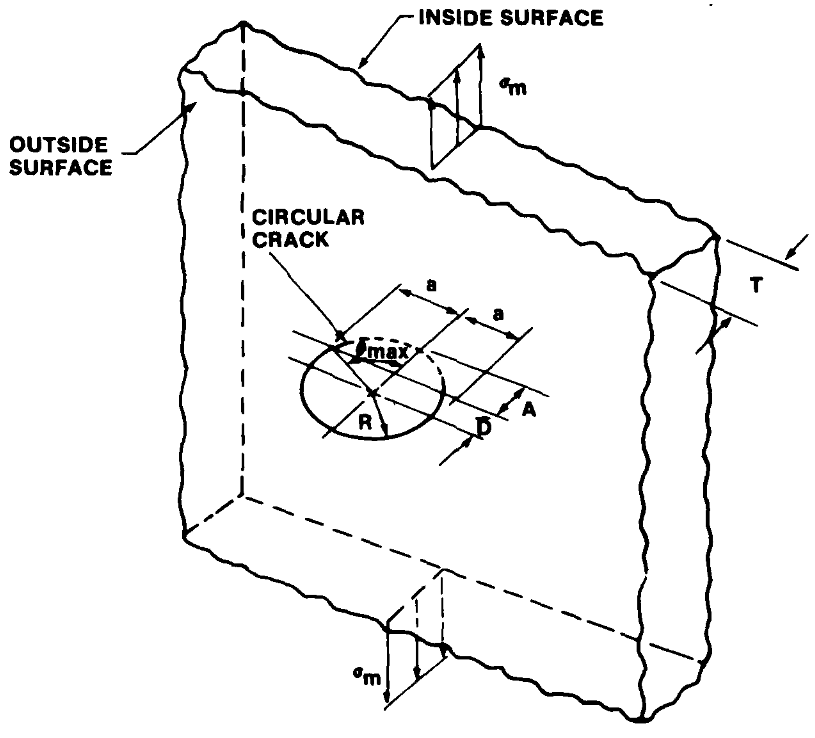

Figure 2. Notation for the part-circular surface flaw.

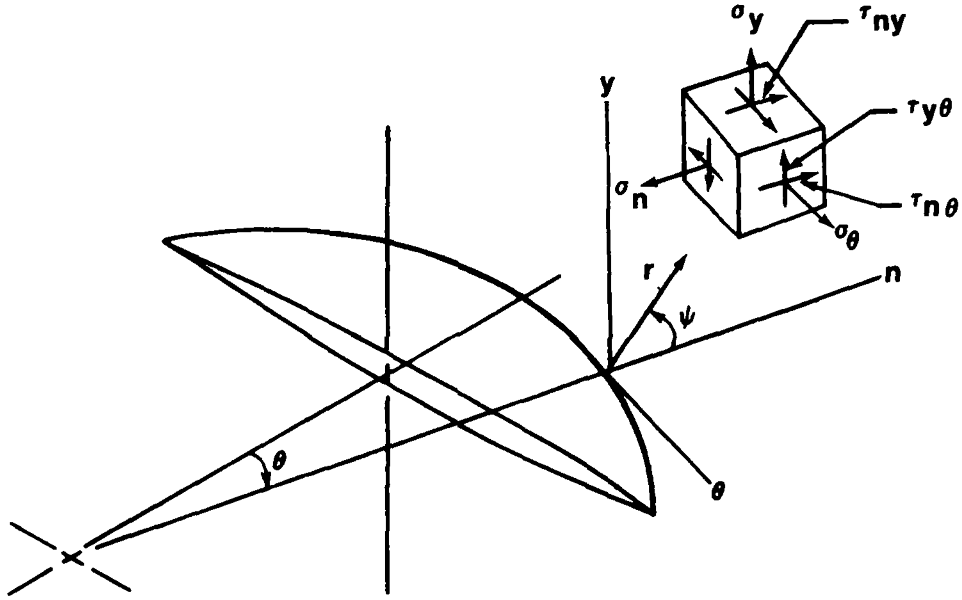

Figure 3. Sketch of crack-tip coordinates.

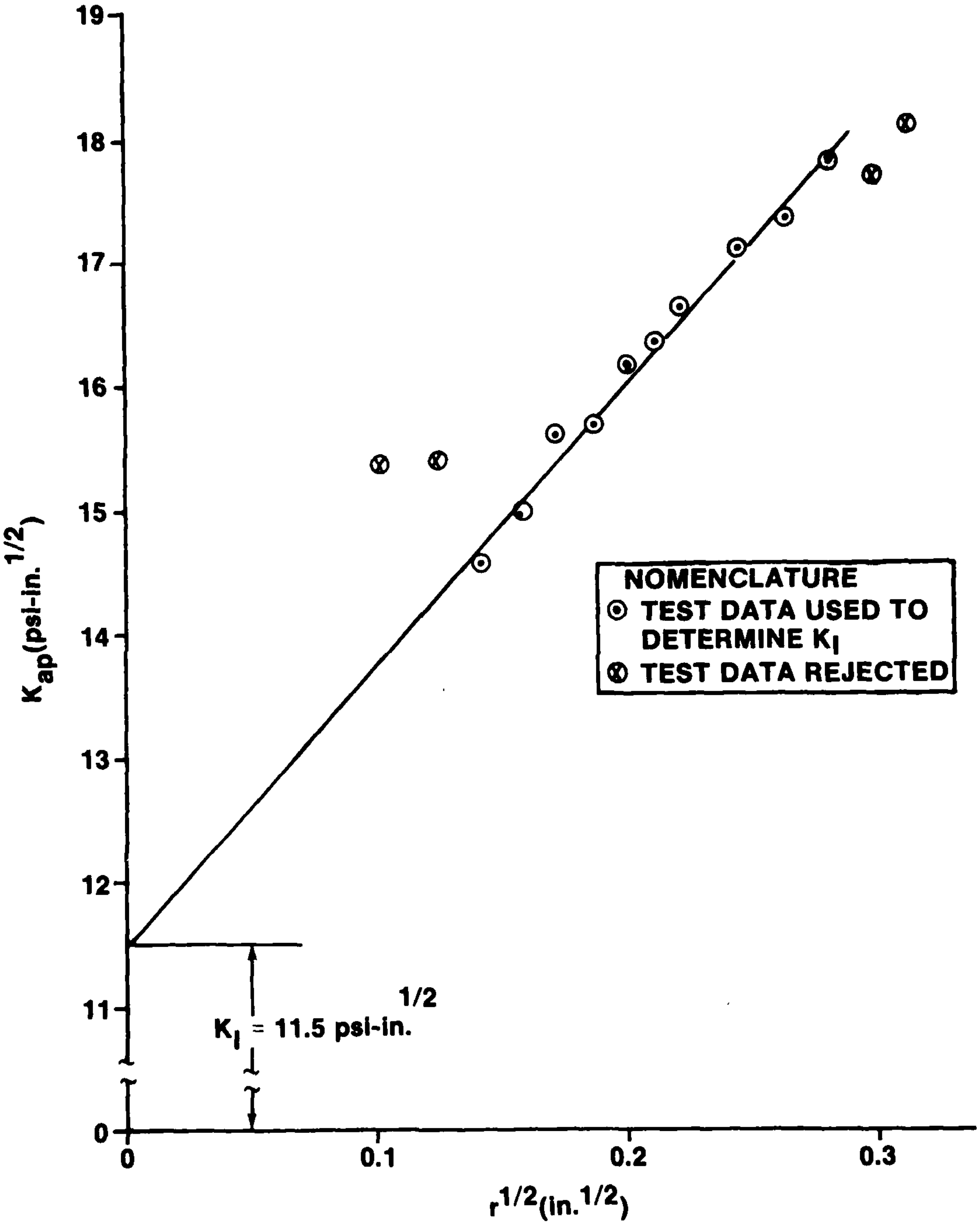

Figure 4. Typical set of slice data, illustrating the determination of K_I.

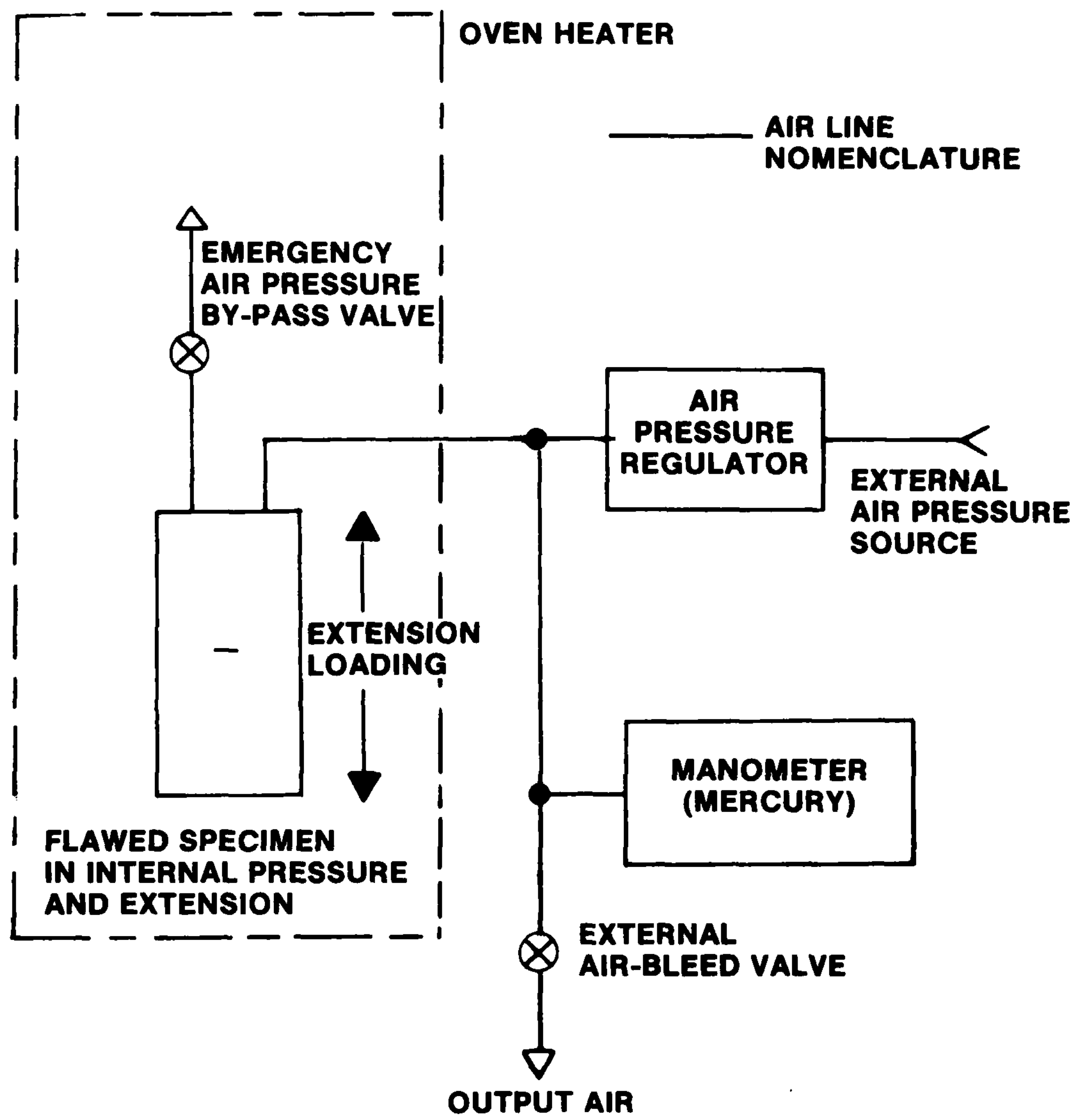

Figure 5. Schematic configuration for internal pressure and/or extension loading of cylinders.

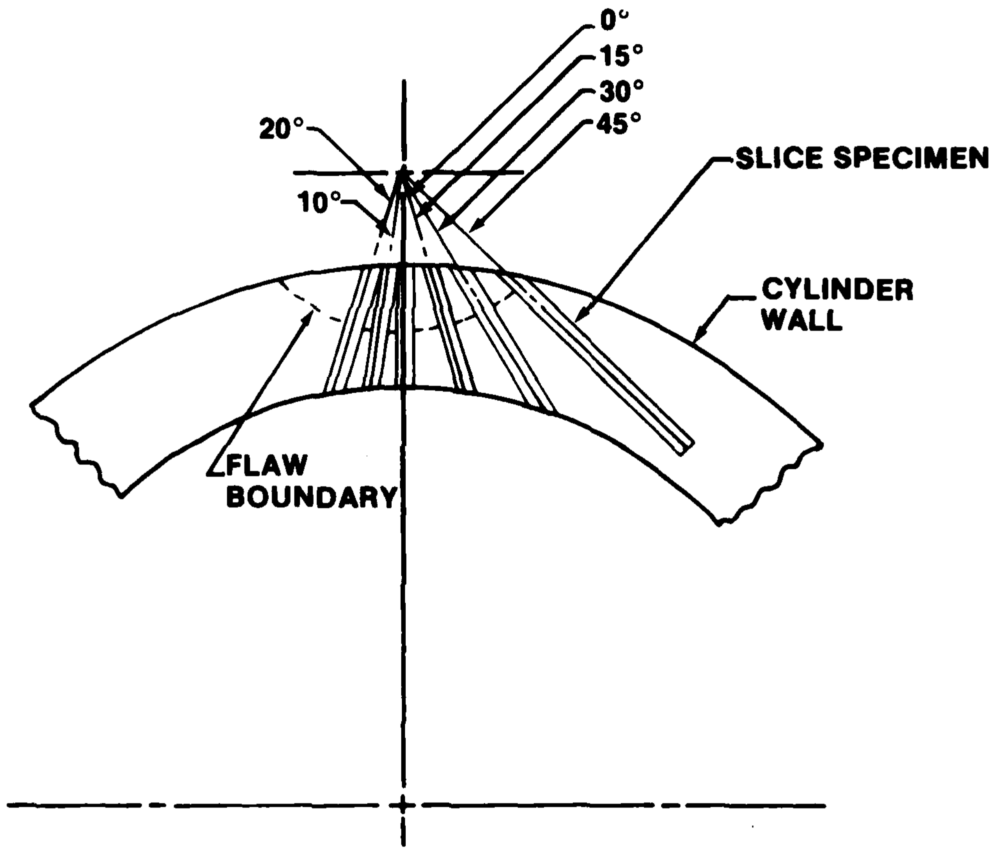

Figure 6. Example slicing scheme for a transverse flaw.

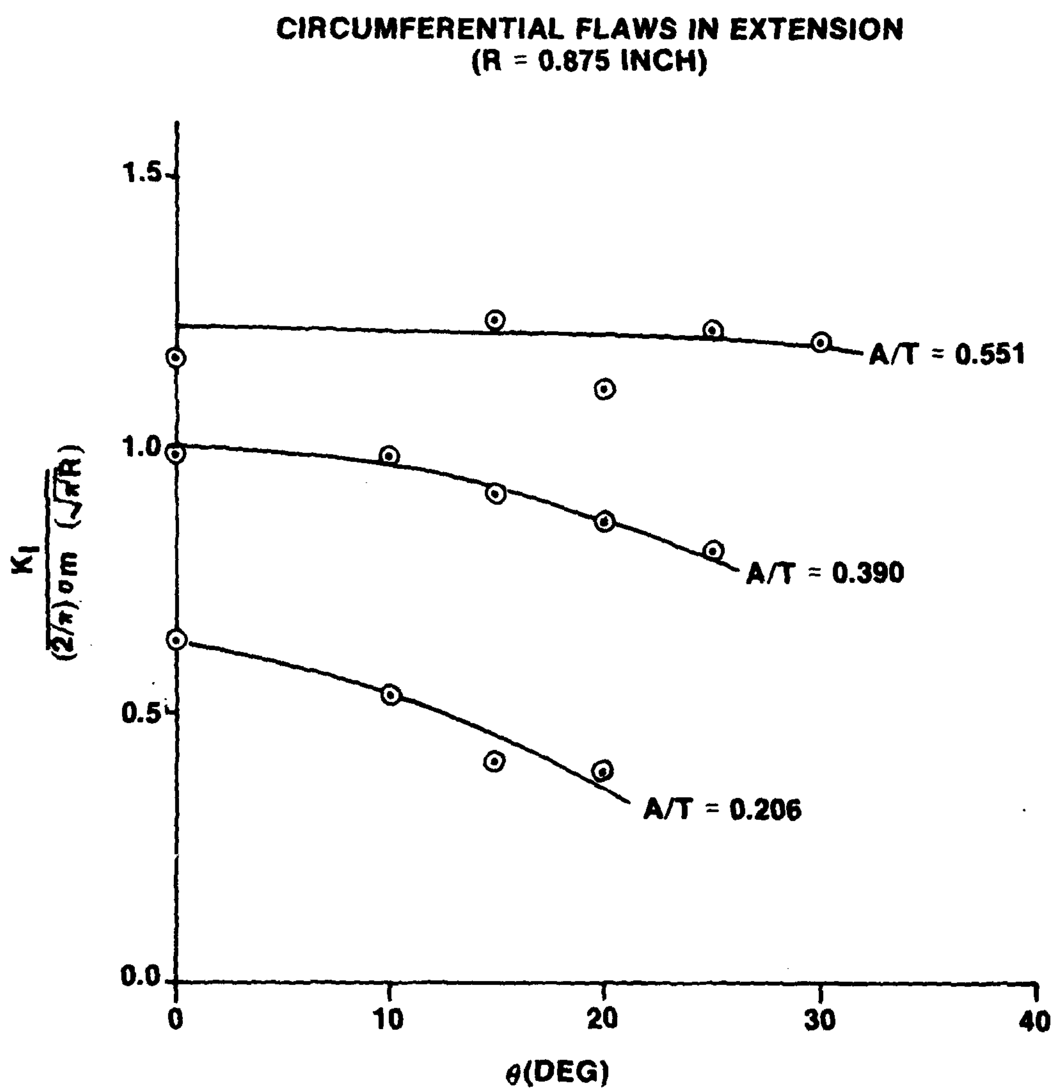

Figure 7. Stress intensity factor versus θ for the transversely-flawed cylinder loaded in uniaxial tension (R = 0.875 inch).

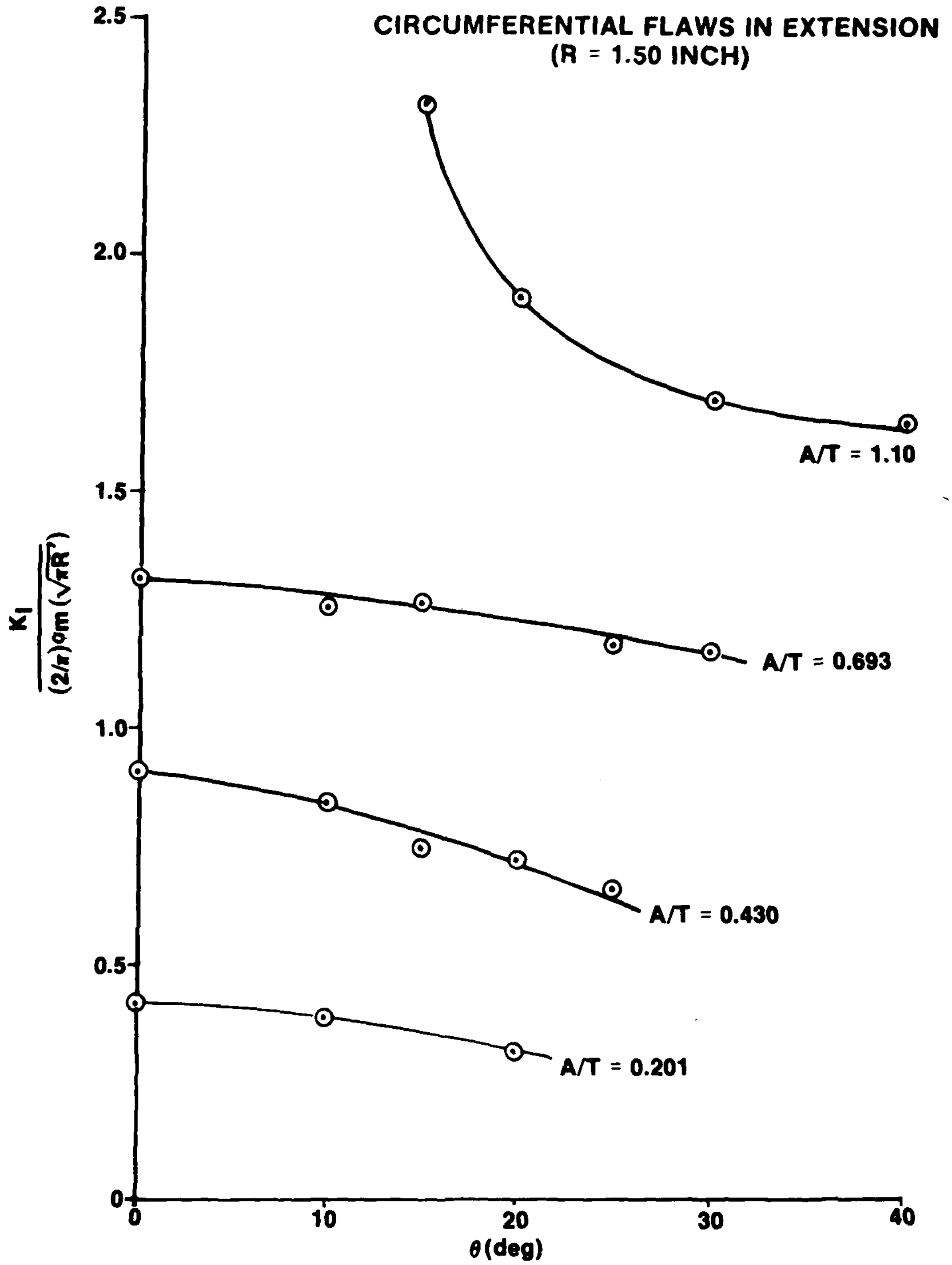

Figure 8. Stress intensity factor versus θ for the transversely-flawed cylinder loaded in uniaxial tension (R = 1.500 inch).

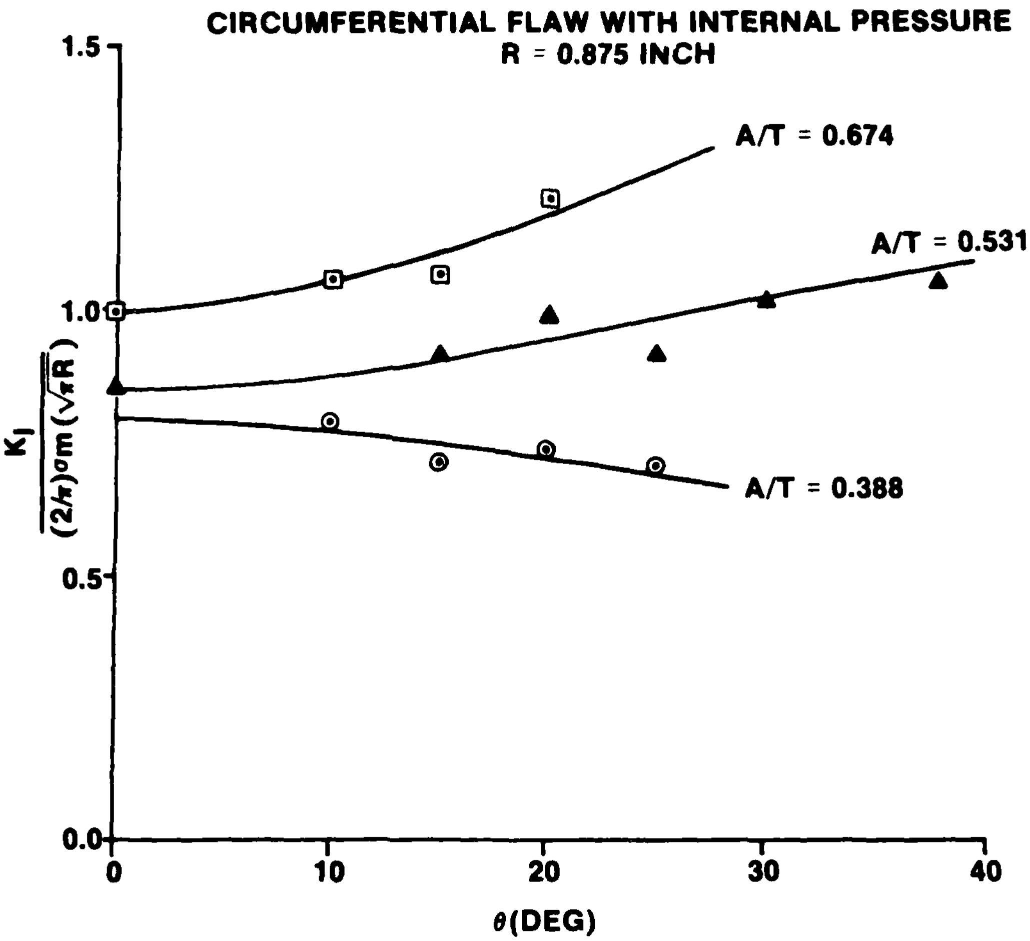

Figure 9. Stress intensity factor versus θ for the transversely-flawed cylinder loaded with internal pressure (R = 0.875 inch).

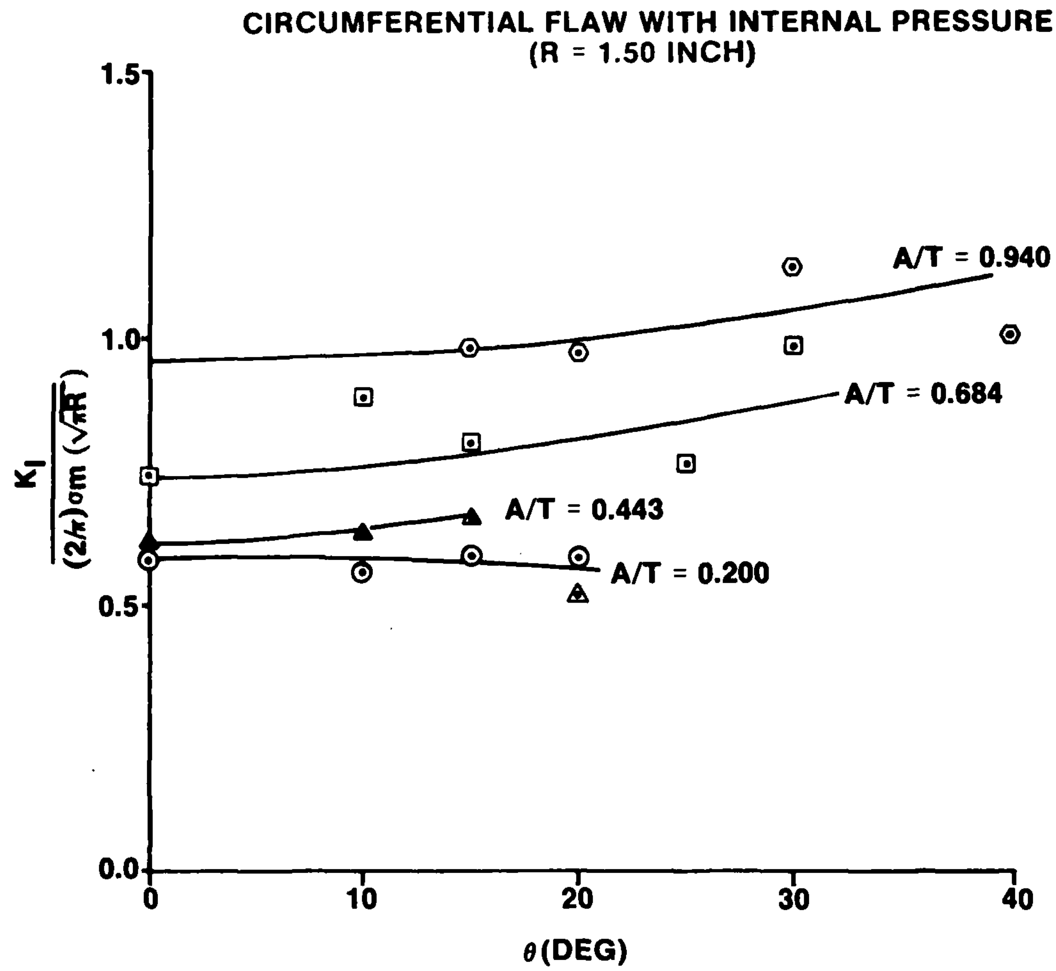

Figure 10. Stress intensity factor versus θ for the transversely-flawed cylinder loaded with internal pressure (R = 1.500 inch).

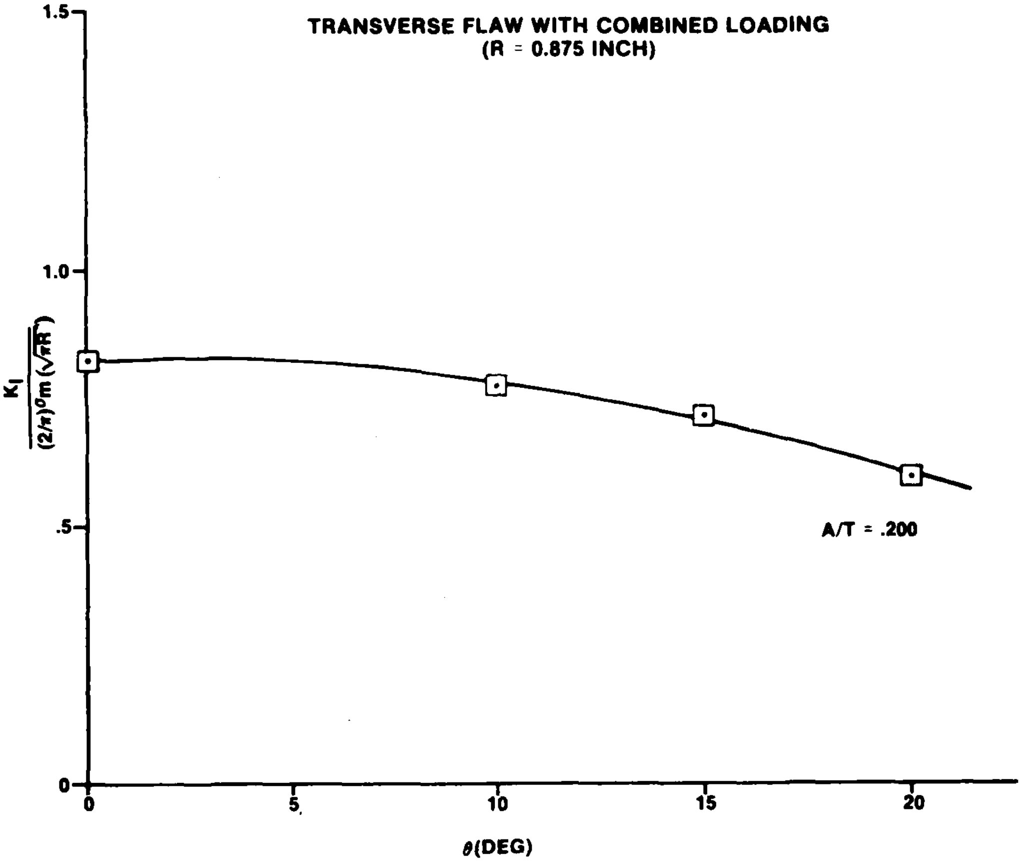

Figure 11. Stress intensity factor versus θ for the transversely-flawed cylinder loaded with internal pressure and extension (R = 0.875 inch, A/T = .200).

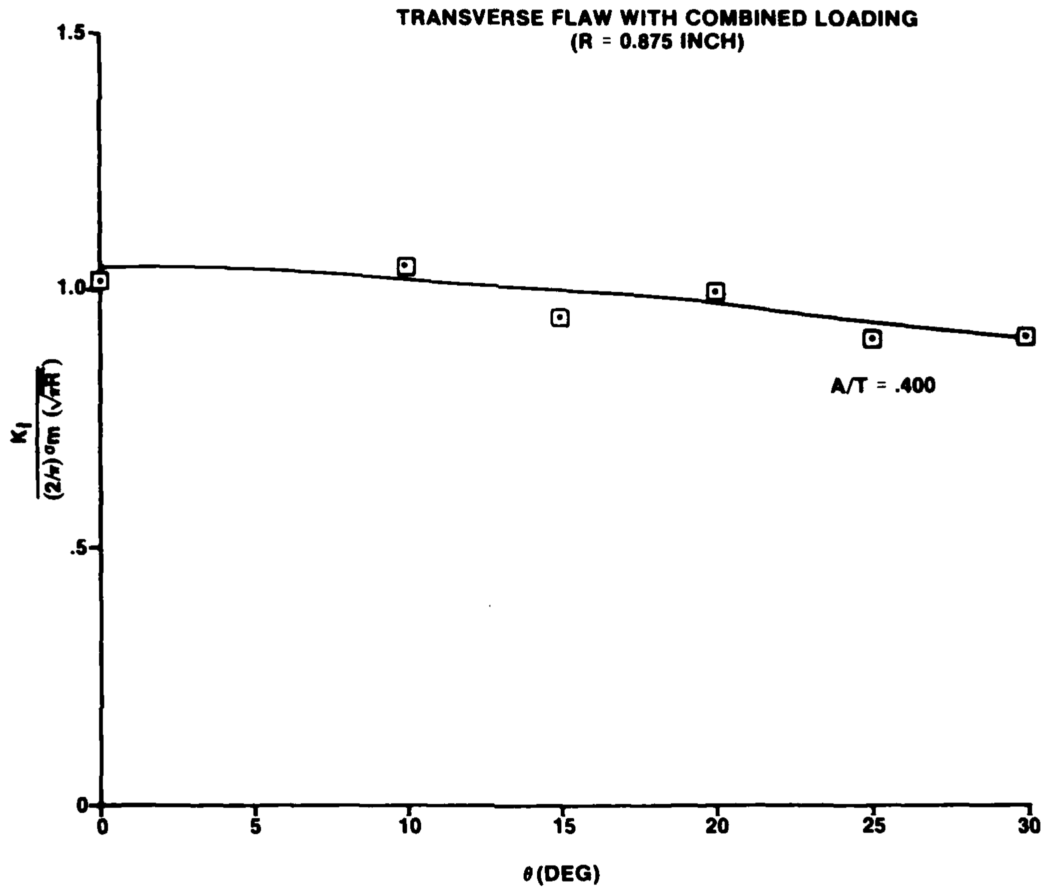

Figure 12. Stress intensity factor versus θ for the transversely-flawed cylinder loaded with internal pressure and extension (R = 0.875 inch, A/T = .400).

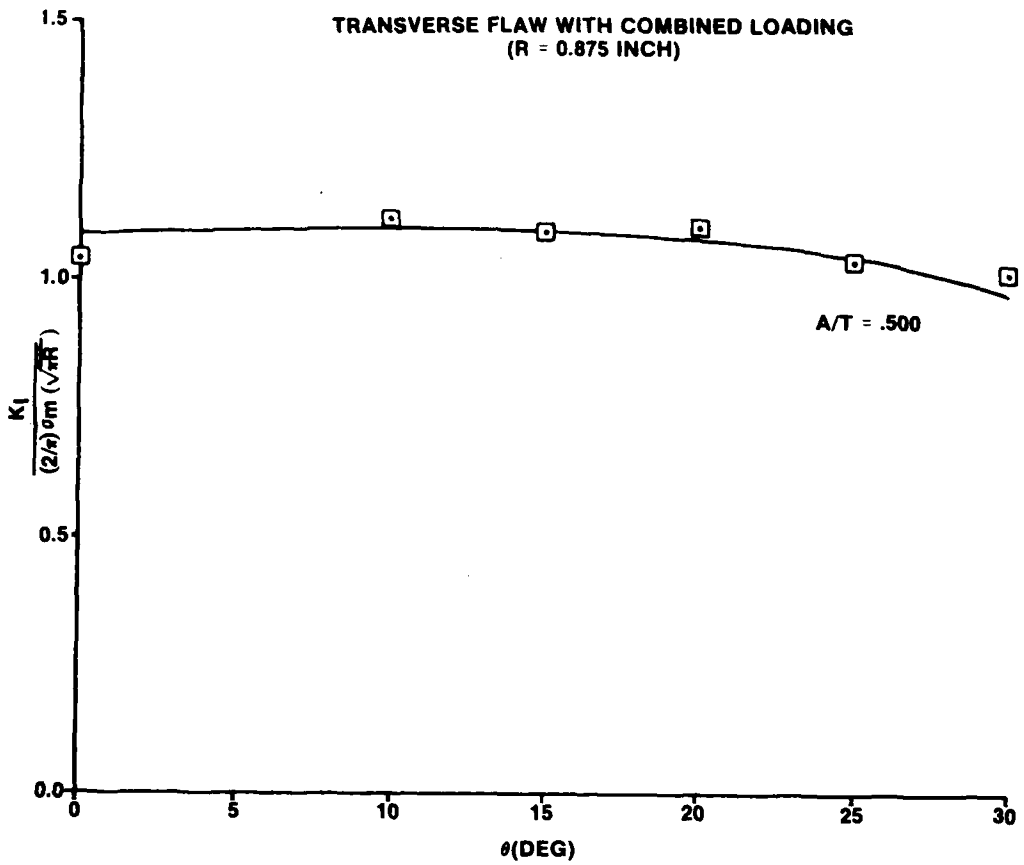

Figure 13. Stress intensity factor versus θ for the transversely-flawed cylinder loaded with internal pressure and extension (R = 0.875 inch, A/T = .500).

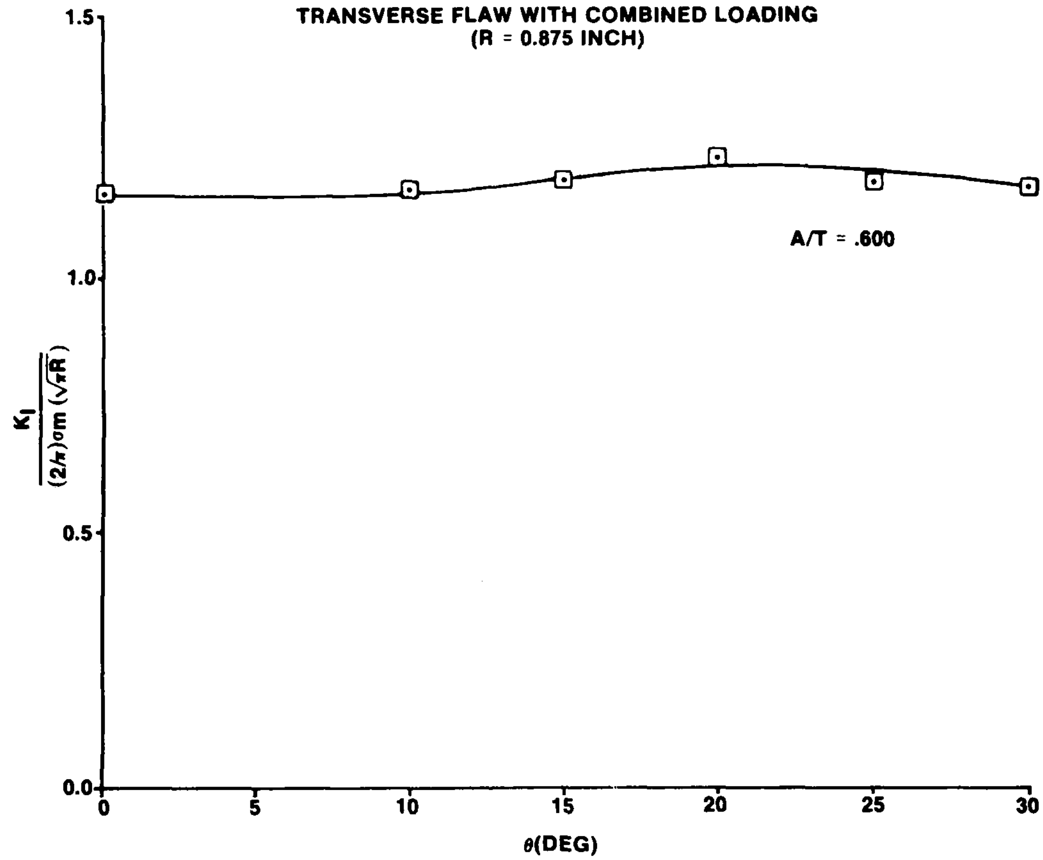

Figure 14. Stress intensity factor versus θ for the transversely-flawed cylinder loaded with internal pressure and extension (R = 0.875 inch, A/T = .600).

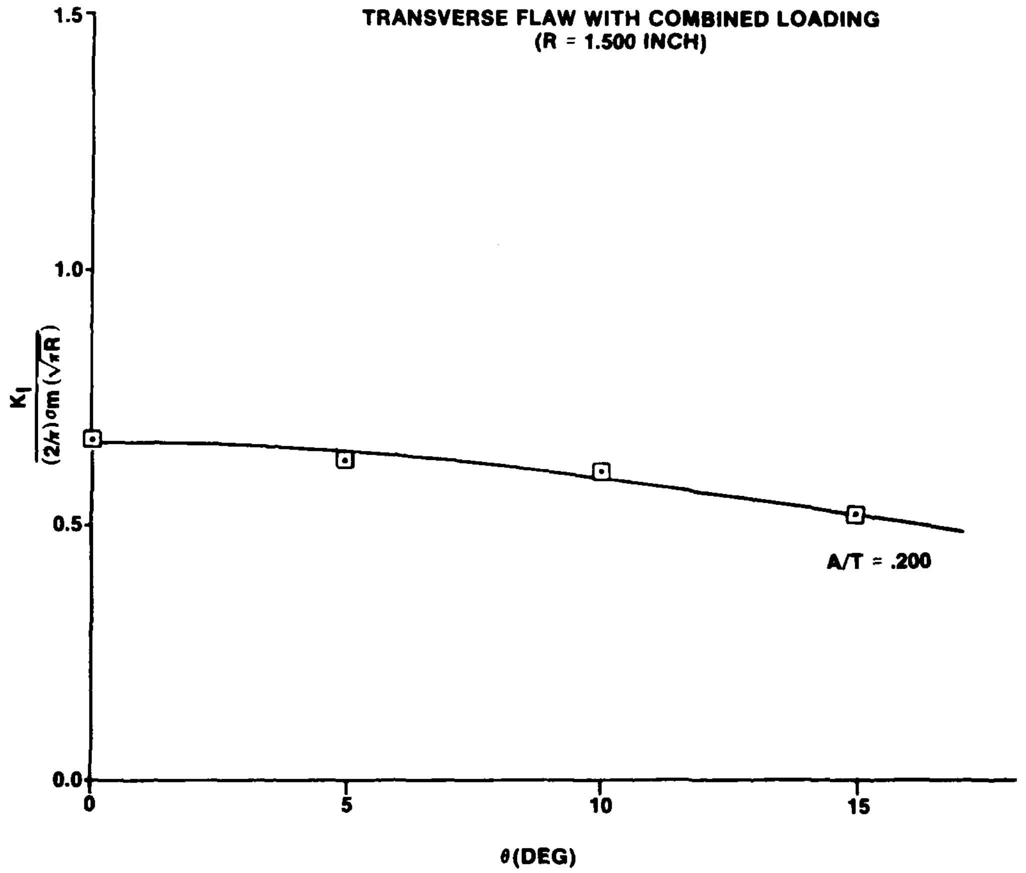

Figure 15. Stress intensity factor versus θ for the transversely-flawed cylinder loaded with internal pressure and extension (R = 1.500, inch, A/T = .200).

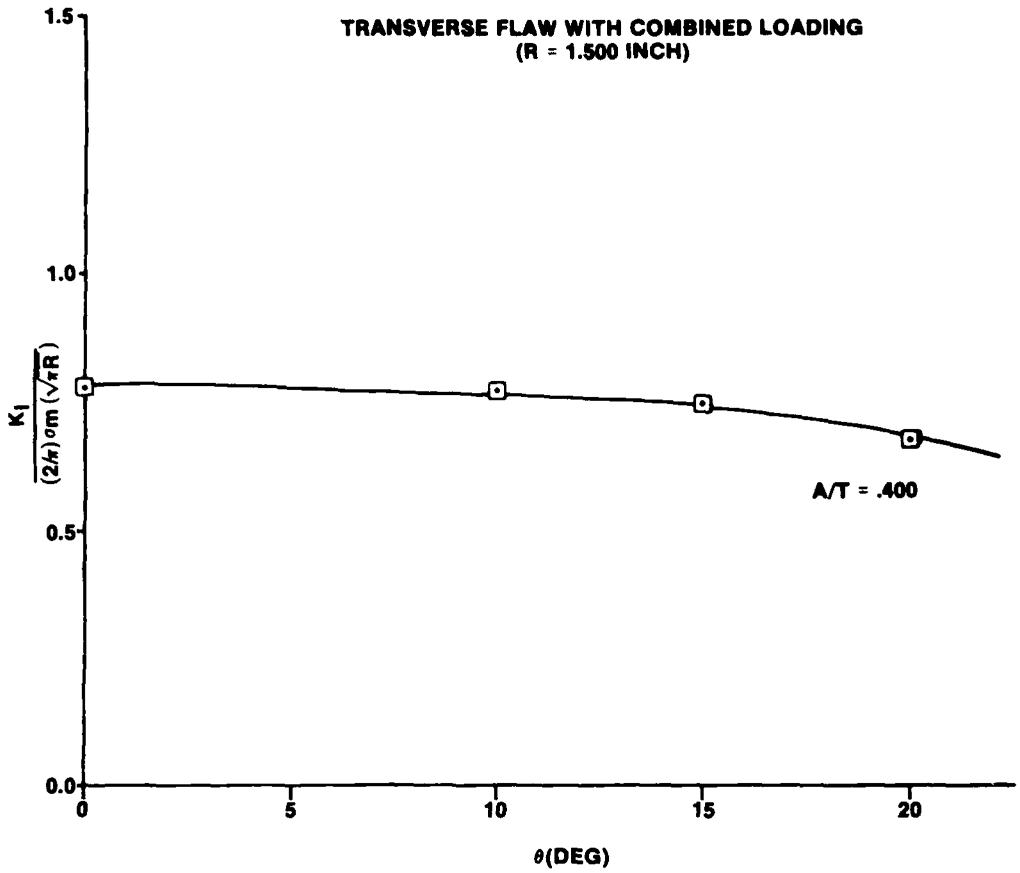

Figure 16. Stress intensity factor versus θ for the transversely-flawed cylinder loaded with internal pressure and extension (R = 1.500 inch, A/T = .400).

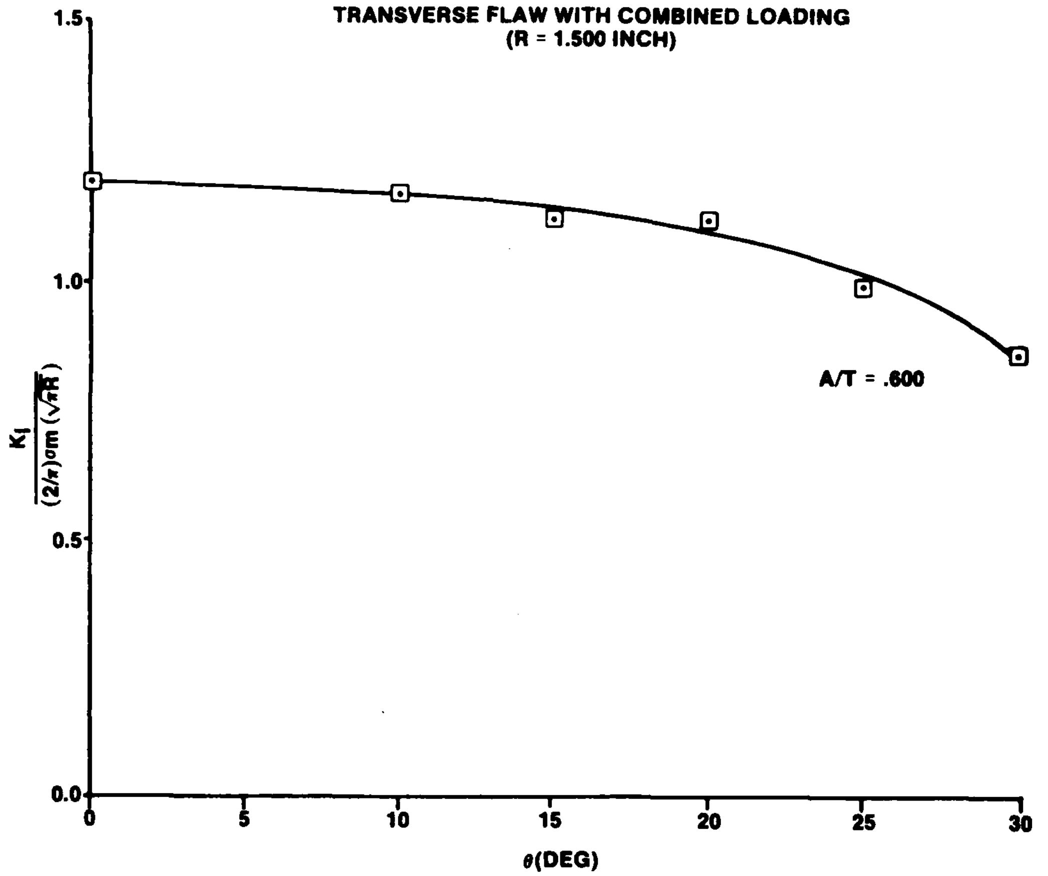

Figure 17. **Stress intensity factor versus θ for the transversely-flawed cylinder loaded with internal pressure and extension (R = 1.500 inch, A/T = .600).**

TABLE 1. SPECIMEN DIMENSIONS AND TEST PARAMETERS FOR TRANSVERSELY-FLAWED CYLINDERS LOADED IN UNIAXIAL TENSION

TEST PARAMETERS	1T	2T	3T	4T	5T	6T	7T	8T
R (inch)	0.88	0.88	0.88	0.88	1.50	1.50	1.50	1.50
T (inch)	0.706	0.724	0.740	0.721	0.721	0.739	0.718	0.725
A (inch)	0.145	0.282	0.408	0.486	0.145	0.318	0.498	0.800
$\bar{D}$ (inch)	0.729	0.593	0.467	0.369	1.355	1.182	1.002	0.700
OD (inch)	5.88	5.86	5.86	5.86	5.86	5.87	5.90	5.86
θ_{max} (degree)	29.5	41.8	51.2	56.6	21.0	30.9	39.3	51.1
2a (inch)	0.865	1.175	1.376	1.480	1.080	1.560	1.935	2.400
D (inch)	0.834	0.678	0.534	0.444	0.903	0.788	0.668	0.467
A/T	0.206	0.390	0.551	0.674	0.201	0.430	0.693	1.100
A/2a	0.168	0.240	0.296	0.328	0.134	0.204	0.257	0.333
d (inch)	3.670	3.523	3.397	3.319	4.280	4.112	3.930	3.630
Load (pound) P	125.33	120.[illegible]3	112.38	115.03	110.38	100.06	94.34	60.37
σ_m (psi) = P/A_c	10.74	10.32	9.72	9.84	9.48	8.42	8.13	5.16
$2/\pi\ \sigma_m(\pi R)^{1/2}$ (psi-inch$^{1/2}$)	11.34	10.90	10.26	10.39	13.12	11.63	11.24	7.14
f (psi-inch)/(fringe)	1.56	1.56	1.56	1.56	1.56	1.56	1.56	1.56
Crack Width (inch)	0.0082	0.0076	0.0082	0.0080	0.0060	0.0062	0.0065	0.0066

TABLE 2. SPECIMEN DIMENSIONS AND TEST PARAMETERS FOR TRANSVERSELY-FLAWED CYLINDERS LOADED WITH INTERNAL PRESSURE

TEST PARAMETERS	1PC	2PC	3PC	4PC	5PC	6PC	7PC	8PC
R (Inch)	Test Failure	0.875	0.875	0.875	1.500	1.500	1.500	1.500
T (Inch)	Test Failure	0.721	0.726	0.724	0.718	0.720	0.718	0.710
A (Inch)	Test Failure	0.279	0.385	0.488	0.144	0.319	0.491	0.668
$\bar{D}$ (Inch)	Test Failure	0.596	0.490	0.387	1.356	1.181	1.009	0.832
OD (Inch)	Test Failure	5.86	5.86	5.86	5.86	5.86	5.86	5.86
θ_{max} (Degree)	Test Failure	41.63	49.52	56.73	20.61	31.05	39.04	45.91
2a (Inch)	Test Failure	1.17	1.34	1.46	1.06	1.55	1.89	2.18
D (Inch)	Test Failure	0.681	0.560	0.442	0.904	0.787	0.673	0.555
A/T	Test Failure	0.388	0.531	0.674	0.200	0.443	0.684	0.940
A/2a	Test Failure	0.238	0.287	0.334	0.136	0.205	0.260	0.306
d (Inch)	Test Failure	3.526	3.421	3.317	4.286	4.111	3.939	3.762
P_i (psi)	Test Failure	3.33	2.98	5.59	6.22	5.56	4.85	4.16
$\sigma_m = (P_i R_c)/(2T)$ (psi)	Test Failure	5.93	5.27	9.91	11.13	9.92	8.68	7.54
$2/\pi\ \sigma_m(\pi R)^{1/2}$ (psi-inch$^{1/2}$)	Test Failure	6.26	5.56	10.46	15.39	13.71	11.99	10.43
f (psi-inch)/fringe	Test Failure	1.56	1.56	1.56	1.56	1.56	1.56	1.56
Crack Width (Inch)	Test Failure	0.0058	0.0068	0.0074	0.0079	0.0071	0.0078	0.0091

TABLE 3. SPECIMEN DIMENSIONS AND TEST PARAMETERS FOR TRANSVERSELY-FLAWED CYLINDERS LOADED IN COMBINED UNIAXIAL TENSION AND INTERNAL PRESSURE

TEST PARAMETERS	1PE	2PE	3PE	4PE	5PE	6PE	7PE
R (Inch)	.875	.875	.875	.875	1.500	1.500	1.500
T (Inch)	.7067	.7306	.7295	.7341	.7303	.7351	.7343
A (Inch)	.141	.292	.365	.440	.146	.294	.440
$\bar{D}$ (Inch)	.734	.583	.510	.435	1.354	1.206	1.060
OD (Inch)	5.88	5.88	5.88	5.88	5.88	5.88	5.88
θ_{max} (Degree)	29.05	42.66	48.20	53.51	20.77	29.78	36.82
2a (Inch)	.850	1.186	1.304	1.407	1.062	1.490	1.798
D	.839	.666	.583	.497	.903	.804	.707
A/T	.200	.400	.500	.600	.200	.400	.600
A/2a	.166	.246	.280	.313	.137	.197	.245
d (Inch)	3.674	3.523	3.450	3.375	4.294	4.146	4.000
Load (pound)	81.29	71.28	64.37	61.30	64.39	54.32	51.36
σ_m (psi)	13.93	11.88	11.17	10.28	10.98	9.94	8.69
P_i (psi)	3.808	3.370	3.160	2.930	3.11	2.93	2.48
f (psi-inch/fringe)	1.56	1.56	1.56	1.56	1.56	1.56	1.56
Crack Width (Inch)	.0071	.0074	.0064	.0064	.0213	.0069	.0061

PRECEDING PAGE BLANK-NOT FILMED

REFERENCES

1. Mullinix, B. R. and Smith, D. G., *An Experimental Determination of the Stress Intensity Around Surface Flaws Embedded in Hollow Cylinders Subjected to Bending*, Technical Report RL-74-7, US Army Missile Command, Redstone Arsenal, Alabama, February 1974.

2. Vandiver, T. L., Schaeffel, J. A., and Smith, D. G., *Stress Intensities Around Surface Flaws in Cylindrical Shells by Stress Freezing*, Technical Report T-79-11, US Army Missile Research and Development Command, Redstone Arsenal, Alabama, 15 December 1978.

3. Kassir, M. and Sil, G. C., "Three-Dimensional Stress Distribution Around an Elliptical Crack Under Arbitrary Loading," *Journal of Applied Mechanics*, Vol. 33, No. 3, September 1966, pp. 601-611.

4. Sneddon, I. N., "The Distribution of Stress in the Neighborhood of a Crack in an Elastic Solid," *Proceedings of the Royal Society*, Series A, Vol. 187, 1946, pp. 229-260.

5. Thresher, R. W. and Smith, F. W., "Stress-Intensity Factors for a Surface Crack in a Finite Solid," *Journal of Applied Mechanics*, Series E, Vol. 39, No. 1, March 1972, pp. 195-200.

6. Irwin, G. R., "Discussion of the Dynamic Stress Distribution Surrounding a Running Crack — A Photoelastic Analysis," *Proceedings, Society for Experimental Stress Analysis*, Vol. 16, No. 1, 1958, pp. 93-96.

7. Smith, C. W., McGowan, J. J., and Peters, W. H., "A Study of Crack-Tip Nonlinearities in Frozen Stress Fields," *Experimental Mechanics*, Vol. 18, No. 8, August 1978.

APPENDIX A

TEST DATA

This appendix contains a summary of all the test data presented in this report. The test nomenclature is as follows:

T ≡ Extension loading test.
PC ≡ Internal pressure loading test.
PE ≡ Combined internal pressure and extension loading test.

The test nomenclature follows the test number. For example, 1PE refers to the first test run of a flaw in the transverse orientation subjected to combined internal pressure and extension loading.

TEST NO. 1T

A/T = 0.206	R = 0.875 inch		σ_m = 10.74 psi
SLICE NO.	ANGLE (DEG)	K_I	$\frac{K_I}{2/\pi\ \sigma_m(\sqrt{\pi R})}$
1	0	7.1788	0.633
2	10	6.0309	0.532
3	15	4.6534	0.410
4	20	4.4673	0.394

TEST NO. 2T

A/T = 0.390	R = 0.875 inch		σ_m = 10.32 psi
SLICE NO.	ANGLE (DEG)	K_I	$\frac{K_I}{2/\pi\ \sigma_m(\sqrt{\pi R})}$
1	0	10.7465	0.986
2	10	10.6959	0.981
3	15	9.9365	0.912
4	20	9.3772	0.860
5	25	8.7716	0.805

TEST NO. 3T

A/T = 0.551	R 0.875 inch		σ_m = 9.72 psi
SLICE NO	ANGLE (DEG)	K_I	$\frac{K_I}{2/\pi\ \sigma_m(\sqrt{\pi R})}$
1	0	11.9434	1.164
2	15	12.6552	1.233
3	20	11.3063	1.102
4	25	12.4901	1.217
5	30	12.2604	1.195

TEST NO. 4T

A/T = 0.674	R = 0.875 inch		σ_m = 9.84 psi
SLICE NO	ANGLE (DEG)	K_I	$\frac{K_I}{2/\pi\ \sigma_m(\sqrt{\pi R})}$
1	0	12.0330	1.158
3	20	14.8617	1.431
4	20	13.7995	1.329
5	30	13.1259	1.264

TEST NO. 5T

A/T = 0.201	R = 1.50 inch		σ_m = 9.48 psi
SLICE NO	ANGLE (DEG)	K_I	$\frac{K_I}{2/\pi\ \sigma_m(\sqrt{\pi R})}$
1	0	5.4174	0.413
2	10	5.1066	0.389
3	20	4.0967	0.312

TEST NO. 6T

A/T = 0.430	R = 1.50 inch		σ_m = 8.416 psi
SLICE NO	ANGLE (DEG)	K_I	$\frac{K_I}{2/\pi\ \sigma_m(\sqrt{\pi R})}$
1	0	10.5044	0.903
2	10	9.8152	0.844
3	15	8.6668	0.745
4	20	8.5062	0.731
5	25	7.6702	0.659

TEST NO. 7T

A/T = 0.693	R 1.50 inch		σ_m = 8.133 psi
SLICE NO	ANGLE (DEG)	K_I	$\frac{K_I}{2/\pi\ \sigma_m(\sqrt{\pi R})}$
1	0	14.8162	1.318
2	10	14.1479	1.258
3	15	14.2745	1.270
4	25	13.2439	1.178
5	30	13.0841	1.164

TEST NO. 8T

A/T = 1.10	R = 1.50 inch		σ_m = 5.162 psi
SLICE NO.	ANGLE (DEG)	K_I	$\frac{K_I}{2/\pi\ \sigma_m(\sqrt{\pi R})}$
1	15	16.5615	2.321
2	20	13.6390	1.912
3	30	12.0614	1.691
4	40	11.7697	1.649

TEST NO. 2PC

A/T = 0.388	R = 0.875 inch		σ_m = 5.93 psi
SLICE NO	ANGLE (DEG)	K_I	$\frac{K_I}{2/\pi\ \sigma_m(\sqrt{\pi R})}$
2	10	4.9448	0.7899
3	15	4.4775	0.7153
4	20	4.6233	0.7385
5	25	4.3932	0.7018

TEST NO. 3PC

A/T = 0.531	R = 0.875 inch		σ_m = 5.27 psi
SLICE NO	ANGLE (DEG)	K_I	$\frac{K_I}{2/\pi\ \sigma_m(\sqrt{\pi R})}$
1	0	4.7515	0.8546
3	15	5.0981	0.9169
4	20	5.4732	0.9844
5	25	5.0620	0.9104
6	30	5.6509	1.0163
7	38	5.8497	1.0521

TEST NO. 4PC

A/T = 0.674	R = 0.875 inch		σ_m = 9.91 psi
SLICE NO.	ANGLE (DEG)	K_I	$\frac{K_I}{2/\pi \ \sigma_m(\sqrt{\pi R})}$
1	0	10.3759	0.9920
2	10	11.0626	1.0576
3	15	11.1789	1.0687
4	20	12.5803	1.2027

TEST NO. 5PC

A/T = 0.200	R = 1.500 inch		σ_m = 11.13 psi
SLICE NO.	ANGLE (DEG)	K_I	$\frac{K_I}{2/\pi \ \sigma_m(\sqrt{\pi R})}$
1	0	9.0737	0.5896
2	10	8.6878	0.5645
3	15	9.1832	0.5967
4	20	9.0818	0.5901

TEST NO. 6PC

A/T = 0.443	R = 1.500 inch		σ_m = 9.92 psi
SLICE NO.	ANGLE (DEG)	K_I	$\frac{K_I}{2/\pi \ \sigma_m(\sqrt{\pi R})}$
1	0	8.4709	0.6179
2	10	8.7018	0.6347
3	15	9.1253	0.6656
4	20	7.0955	0.5175

TEST NO. 7PC

A/T = 0.684	R = 1.500 inch		σ_m = 8.68 psi
SLICE NO.	ANGLE (DEG)	K_I	$\frac{K_I}{2/\pi \ \sigma_m(\sqrt{\pi R})}$
1	0	8.9268	0.7445
2	10	10.6402	0.8874
3	15	9.6247	0.8027
4	25	9.2004	0.7673
5	30	11.8390	0.9874

TEST NO. 8PC

A/T = 0.940	R = 1.500 inch		σ_m = 7.54 psi
SLICE NO.	ANGLE (DEG)	K_I	$\frac{K_I}{2/\pi \ \sigma_m(\sqrt{\pi R})}$
1	15	10.2689	0.9845
2	20	10.1580	0.9739
3	30	11.8707	1.1381
4	40	10 4856	1.0053

TEST NO. 1PE

A/T = 0.200	R = .875 inch		σ_m = 13.93 psi
SLICE NO.	ANGLE (DEG)	K_I	$\frac{K_I}{2/\pi \ \sigma_m(\sqrt{\pi R})}$
1-1	0°	12.1381	.826
1-2	10°	11.3646	.773
1-3	15°	10.4009	.707
1-4	20°	8.7351	.594

TEST NO. 2PE

A/T = .400	R = .875 inch		σ_m = 11.88 psi
SLICE NO.	ANGLE (DEG)	K_I	$\frac{K_I}{2/\pi \ \sigma_m(\sqrt{\pi R})}$
2-1	0°	12.7124	1.014
2-2	10°	13.1542	1.049
2-3	15°	11.8315	.944
2-4	20°	12.5060	.997
2-5	25°	11.3443	.905
2-6	30°	11.3930	.909

TEST NO. 3PE

A/T = .500	R = .875 inch		σ_m = 11.165 psi
SLICE NO.	ANGLE (DEG)	K_I	$\frac{K_I}{2/\pi \ \sigma_m(\sqrt{\pi R})}$
3-1	0°	12.2987	1.044
3-2	10°	13.0904	1.111
3-3	15°	12.9064	1.095
3-4	20°	12.9740	1.101
3-5	25°	12.1957	1.035
3-6	30°	11.9617	1.015

TEST NO. 4PE

A/T .600	R .875 inch		σ_m = 10.28 psi
SLICE NO	ANGLE (DEG)	K_I	$\frac{K_I}{2/\pi\ \sigma_m(\sqrt{\pi R})}$
4-1	0°	12.5119	1.153
4-2	10°	12.6121	1.162
4-3	15°	12.8565	1.185
4-4	20°	13.3028	1.226
4-5	25°	12.8078	1.180
4-6	30°	12.7277	1.173

TEST NO. 5PE

A/T = .200	R = 1.500 inch		σ_m = 10.98 psi
SLICE NO.	ANGLE (DEG)	K_I	$\frac{K_I}{2/\pi\ \sigma_m(\sqrt{\pi R})}$
5-1	0°	10.0986	.666
5-2	5°	9.5187	.627
5-3	10°	9.1719	.604
5-4	15°	7.9137	522

TEST NO. 6PE

A/T = .400	R = 1.500 inch		σ_m = 9.94 psi
SLICE NO.	ANGLE (DEG)	K_I	$\frac{K_I}{2/\pi\ \sigma_m(\sqrt{\pi R})}$
6-1	0°	10 6769	777
6-2	10°	10 6978	.779
6-3	15°	10 2661	747
6-4	20°	9 2705	675

TEST NO. 7PE

A/T = .600	R = 1.500 inch		σ_m = 8.69 psi
SLICE NO.	ANGLE (DEG)	K_I	$\frac{K_I}{2/\pi\ \sigma_m(\sqrt{\pi R})}$
7-1	0°	14.4033	1.199
7-2	10°	13.8254	1.151
7-3	15°	13 5577	1.129
7-4	20°	13 5130	1.125
7-5	25°	11 4605	.954
7-6	30°	10 3812	.864

APPENDIX B

COMPUTER CODE

The computer code shown on the following pages was used to analyze the photoelastic data. The code uses the technique presented in Section II. With at least squares straight-line curve fit of the experimental data.

```
C--------------PHOTOELASTICITY CODE-CYLINDERS
      DIMENSION AN(50),AR(50),AT(50),AK(50),ID(50)
      WRITE(5,22)
22    FORMAT('  NO. OF SLICES?')
      READ(5,1) N
1     FORMAT(I3)
      DO 19 I=1,N,1
      M=14
      F=1.56
      WRITE(5,25)
25    FORMAT('  SLICE THICKNESS?')
      READ(5,26) T
26    FORMAT(F10.0)
      WRITE(5,27)
27    FORMAT('  INPUT N-F6.0')
      DO 4 J=1,M,1
      READ(5,3) AN(J)
3     FORMAT(F6.0)
      IF(J.LE.9) AR(J)=FLOAT(J-1)*.005+.010
      IF(J.GT.9) AR(J)=FLOAT(J-9)*.010+.050
4     CONTINUE
      AMAX=0.
      DO 5 J=1,M,1
      AT(J)=F*AN(J)/(2.*T)
      AK(J)=AT(J)*SQRT(8.*3.14159*AR(J))
      IF(AK(J).GT.AMAX) AMAX=AK(J)
5     AR(J)=SQRT(AR(J))
6     CALL IPOKE("170410,"1)
      CALL IPOKE("170410,"0)
      DO 7 J=1,M,1
      IY=INT(AK(J)*1000./AMAX)
      IX=INT(AR(J)*1000./AR(M))
      CALL IPOKE("170412,IX)
      CALL IPOKE("170414,IY)
7     CALL IPOKE("170414,"0)
      ITEST=IPEEK("177570)
      IF(ITEST.EQ.0) GOTO 6
      WRITE(5,8)
```

```
8       FORMAT('  NO. OF DELETE SAMPLES?')
        READ(5,9) ND
9       FORMAT(I3)
        IF(ND.EQ.0) GOTO 20
        DO 11 J=1,ND,1
        READ(5,10) ID(J)
10      FORMAT(I3)
11      CONTINUE
20      CONTINUE
        X1=0.
        X2=0.
        Y0=0.
        Y1=0.
        DO 14 J=1,M,1
        IF(ND.EQ.0) GOTO 21
        DO 13 K=1,ND,1
13      IF(J.EQ.ID(K)) GOTO 14
21      X1=X1+AR(J)
        X2=X2+AR(J)**2.
        Y0=Y0+AK(J)
        Y1=Y1+AK(J)*AR(J)
14      CONTINUE
        AK1=(X2*YO-Y1*X1)/(FLOAT(M-ND)*X2-X1*X1)
        WRITE(5,15) I
15      FORMAT('   SLICE NO. =',I3)
        DO 18 J=1,M,1
        AR(J)=AR(J)**2.
        WRITE (5,16) AR(J),AN(J),AT(J),AK(J)
16      FORMAT('   R=',F10.4,5X,'N='F10.4,5X,
        1'TMAX=',F10.4,5X,'KAPP='F10.4)
18      CONTINUE
        WRITE(5,17) AK1
17      FORMAT('   K1=',F14.4)
19      CONTINUE
        STOP
        END
```

LIST OF SYMBOLS

A	Crack depth at deepest point (semi-minor diameter for elliptical flaw)
A_c	Nominal cross-sectional area of cylinder
a	Half-length of crack on outside surface of wall
$\overline{D}$	Distance from center of circular flaw to surface of the wall
D	Ratio of Distance $\overline{D}$ to radius of circular flaw R
d	Distance from center of cylinder to center of circular flaw
f	Photoelastic fringe constant
K_I, S_{IF}	Mode I stress intensity factor
N	Isochromatic fringe order
P	Total load on cylinder loaded in tension
P_i	Internal cylinder pressure
R	Radius of circular flaw
R_c	Radius of cylinder measured to center of cylinder wall
r, ψ	Polar coordinates centered at crack tip
T	Wall thickness of the cylinder
t	Thickness of a slice analyzed
y, n, θ	Coordinate system shown in *Figure 3*
σ_m	Nominal cylinder-wall stress
σ_{on}	Uniform stress at the crack tip
$\sigma_y, \sigma_n, \sigma_\theta$	Normal stress components
$\tau_{ny}, \tau_{n\theta}, \tau_{y\theta}$	Shear stress components
τ_{max}	Maximum shearing stress in the plane perpendicular to the crack border
θ_{max}	Maximum flaw angle (*Figure 2*)

DISTRIBUTION

	No. of Copies
Headquarters SAC/NRI (Stinfo Library) Offutt Air Force Base, Nebraska 68113	1
Commander (Code 233) Naval Weapons Center ATTN: Library Division China Lake, California 93555	1
Department of the Army US Army Research Office ATTN: Information Processing Office P. O. Box 12211 Research Triangle Park, North Carolina 27709	1
ADTC (DLDSL) Eglin Air Force Base, Florida 32542	1
University of California Los Alamos Scientific Laboratory ATTN: Reports Library P. O. Box 1663 Los Alamos, New Mexico 87545	1
Library US Army War College Carlisle Barracks, Pennsylvania 17013	1
Tennessee Technological University Department of Engineering Science ATTN: Dallas G. Smith Cookeville, Tennessee 38501	1
Defense Technical Information Center Cameron Station Alexandria, Virginia 22314	12

DISTRIBUTION (Continued)

	No. of Copies
Defense Metals Information Center Battelle Memorial Institute 505 King Avenue Columbus, Ohio 43201	1
Commander US Army Foreign Science and Technology Center ATTN: DRXST-SD3 220 Seventh Street, NE Charlottesville, Virginia 22901	1
Office of Chief of Research and Development Department of the Army ATTN: DARD-ARS-P Washington, DC 20301	1
Commander US Army Natick Laboratories Kansas Street ATTN: STSNLT-EQR Natick, Massachusetts 01760	1
Commander US Army Mobility Equipment Research and Development Center Fort Belvoir, Virginia 22060	1
Commander Edgewood Arsenal ATTN: SAREA-TS-A Aberdeen Proving Ground, Maryland 21010	1
Commander Picatinny Arsenal ATTN: SARPA-TS-S, Mr. M. Costello Dover, New Jersey 07801	1
Commander Watervliet Arsenal Watervliet, New York 12189	1
Commander US Army Test and Evaluation Command ATTN: DRSTE-RA Aberdeen Proving Ground, Maryland 21005	1

DISTRIBUTION (Continued)

	No. of Copies
Director Air Force Materiel Laboratory ATTN: APML-DO-Library Wright-Patterson AFB, Ohio 45433	 1
Director, Army Materials and Mechanics Research Center ATTN: DRXMR-PL -MT, Mr. Farrow Watertown, Massachusetts 02172	 1 1
Technical Library Naval Ordnance Station Indian Head, Maryland 20640	 1
Commander US Army Materiel Development and Readiness Command ATTN: DRCMT Washington, DC 20315	 1 1
US Army Research and Standardization Group (Europe) ATTN: DRXSN-E-RX, Dr. Alfred K. Nedoluha Box 65 FPO New York 09510	 2
US Army Materiel Development and Readiness Command ATTN: Mr. Edward Sedlak Dr. James Bender 5001 Eisenhower Avenue Alexandria, Virginia 22333	 1 1
Headquarters, Department of the Army Office of the Deputy Chief of Staff for Research and Development and Acquisition ATTN: DAMA-ARZ Room 3A474, Pentagon Washington, DC 20310	 2
Director Defense Research and Engineering ATTN: Mr. Leonard R. Weisberg Room 3D1079, Pentagon Washington, DC 20301	 2

DISTRIBUTION (Concluded)

	No. of Copies
Director Defense Advanced Research Projects Agency 1400 Wilson Boulevard Arlington, Virginia 22209	1
Commander US Army Research Office ATTN: DRXRO-PH, Dr. R. Lontz P. O. Box 12211 Research Triangle Park, North Carolina 27709	2
IIT Research Institute ATTN: GACIAC 10 West 35th Street Chicago, Illinois 60616	1
US Army Materiel Systems Analysis Activity ATTN: DRXSY-MP Aberdeen Proving Ground, Maryland 21005	1
DRSMI-LP , Mr. Voigt	1
-R , Dr. Kobler	1
-RL , Mr. Comus	1
-RLA, Mr. Pettey	1
Mr. Schaeffel	50
-RPR	3
-RPT (Record Set)	1
-RPT (Reference Copy)	1